RSC Advances

ROYAL SOCIETY OF CHEMISTRY

www.rsc.org/advances

Surface-Dependence of Interfacial Binding Strength between Zinc Oxide and Graphene

Kelsey Larson,[1] Adam Clark,[1] Allyse Appel,[1] Qingli Dai,[2] Haiying He,[1,a)] and Stan Zygmunt[1]

[1]*Department of Physics and Astronomy, Valparaiso University, Valparaiso, IN 46383*

[2]*Department of Civil and Environmental Engineering, Michigan Technological University, Houghton, MI 49931*

ABSTRACT

There is an increasing interest in hybrid materials with impacts such as improving structural integrity of known and commonly used materials. Recent experiments have suggested that the adhesion of zinc oxide (ZnO) nanowires with carbon fibers can significantly improve interfacial shear and tensile strength of fiber reinforced polymer composites. We have carried out a systematic study of the interaction between ZnO and graphene based on density functional theory, with a focus on the effect of the surface orientation and termination of ZnO. The interaction has been explored through varying both the orientation and binding sites of the interacting surfaces. The calculated binding strength shows a strong dependence on the surface orientation and termination of ZnO, which can be explained from the difference in electronegativity of Zn and O, and the induced charge redistribution owing to the in-plane and out-of-plane dipole moment of the oxide surface.

[a)] Author to whom correspondence should be addressed. Electronic mail: haiying.he@valpo.edu

I. INTRODUCTION

Hybrid materials with two or more different components interfaced with each other can provide a significant advantage over their individual components in terms of their physical and chemical properties. The performance of such a material can be superior to the simple algebraic average of the properties of the individual materials, largely owing to the new chemical and physical properties of the interfaces formed between dissimilar materials. This becomes a more important question as low-dimensional and high specific surface area materials are widely adopted in the form of nanocomposites in current research and technological applications. It is recently reported that adding zinc oxide (ZnO) nanowires into the carbon fiber reinforced composites as an interphase between the carbon fibers and the polymer matrix improves the interfacial shear strength of the composites by more than two times.[1] It is believed that the adhesion of ZnO nanowires to carbon fibers plays a critical role in producing the resultant superior mechanical property. In addition, the interesting interplay of electron redistribution at the interface can also lead to better catalytic properties. Researchers have revealed enhanced degradation of RhB dye with a ZnO-graphene composite compared to ZnO or graphene alone.[2] The interest in the ZnO-graphene system goes far beyond photocatalysts,[2-4] and the applications extend to electronic and optoelectronic systems,[5-7] and chemical sensors.[8,9] Substantial efforts are also being made to synthesize such hybrid materials.[10,11]

Interfaces play a key role in these applications, and a detailed understanding of the interaction at the interface of oxides with graphene or graphitic material is crucial towards improving the properties of hybrid materials. Galan *et al.*[12] first studied the interfacial energy between ZnO and graphene by molecular dynamics simulations. In their model, the interaction between ZnO and graphene is described by a Lennard-Jones (L-J) potential. In spite of the fact that L-J potentials are generally adopted for non-bonded interactions, in this case the L-J parameters were crudely approximated by taking the elemental values for carbon and Zn, and then applying the Lorentz–Berthelot mixing rules. Therefore, only one type of van der Waals interaction, namely the London dispersion force, is taken into account. The main

limitation of this classical MD force potential is the omission of the large difference in the electronegativity of Zn and O, which in turn produces highly charged ionic species of these two elements in the oxide. The arrangement of the ions in space may have a dramatic effect on the ability of ZnO to interact with graphitic materials, dominated by highly deformable π electrons. There are only a few first-principles theoretical studies of the structural and electronic properties of graphene-ZnO interfaces, and the focus was on the (001) surface of ZnO in the wurtzite phase.[13,14]

On the other hand, it is notable that many of the fabricated nanostructures of ZnO show the dominant growth along the <001> direction and the preference for the (100) and (110) surfaces and their family surfaces on the facets.[15-18] By tuning the growth kinetics, Wang *et al*. have also shown the possibility of forming a diverse group of ZnO nanostructures, including nanocombs, nanosaws, nanosprings, nanorings, nanobows, and nanopropellers with all kinds of termination surfaces.[19] Generally, the non-polar surfaces such as (100) and (110) are found to be more stable than the polar (001) surfaces. The (110) surface is found to be the most stable for both ZnO and ZnS semiconductors, and the (100) surface is found to have a slightly larger surface energy. These are consistent with the abundant observations of ZnO nanostructures having (110) and (100) surfaces.[20]

The main objective of the present work is to investigate the effect of the surface orientation and termination of ZnO on its interaction with graphene, as a model for a graphitic material with zero curvature. In this work, we have conducted molecular modeling and simulation based on density functional theory (DFT) to calculate the interaction strength, charge redistribution and transfer at the graphene-ZnO interfaces. The thermodynamically most stable hexagonal (wurtzite) phase of ZnO is modeled by a cluster with (001), (100), and (110) facets, and the (001) surface is constructed to have both Zn-rich and O-rich terminations. The interaction has been explored through varying both the orientation and binding sites of the interacting surfaces. The interfacial binding strength is calculated by scanning the potential energy surface while bringing the ZnO cluster incrementally closer to graphene.

II. COMPUTATIONAL METHODS

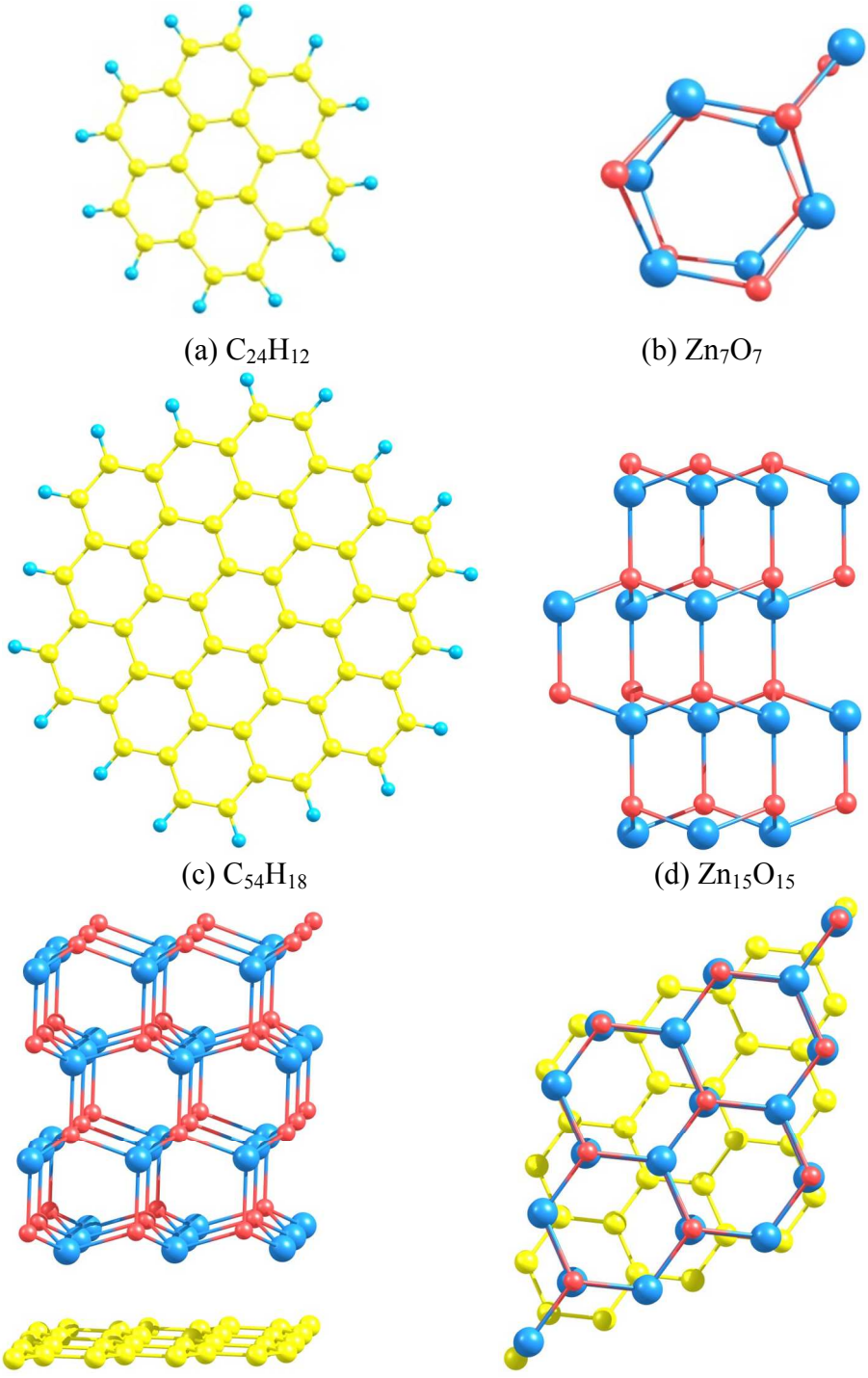

(a) $C_{24}H_{12}$ (b) Zn_7O_7

(c) $C_{54}H_{18}$ (d) $Zn_{15}O_{15}$

(e) PBC: Zn-(001) - Graphene (side view) (f) PBC: Zn-(001) - Graphene (top view)

FIG. 1. Cluster model 1 (CM1) and 2 (CM2) for (a), (c) graphene and (b), (d) zinc oxide in the wurtzite phase; slab model applying the periodic boundary conditions (PBC) for 3×3 ZnO (001) - 4×4 Graphene with (e) side and (f) top views. Symbols: C in yellow, H in light blue, O in red and Zn in navy blue.

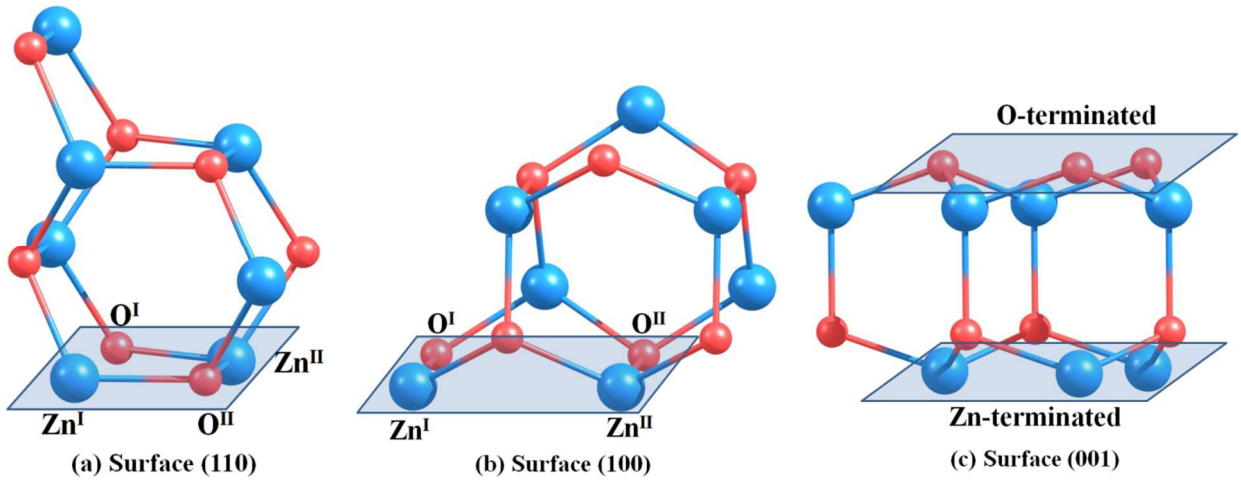

FIG. 2. Low index surfaces of wurtzite ZnO modeled by a Zn_7O_7 cluster. Atomic labels are denoted as Zn^I: 2-fold Zn; Zn^{II}: 3-fold Zn; O^I: 2-fold O; O^{II}: 3-fold O.

The simulations were done by using cluster models for ZnO and graphene. The graphene is modeled by a planar honeycomb structure consisted of seven and nineteen rings for Cluster Model 1 (CM1) and 2 (CM2), respectively, (see Figs. 1a and 1c). The carbon atoms at the edge are terminated by hydrogen atoms to saturate the dangling bonds. As reported in earlier studies,[17,21] most ZnO nanostructures are found to maintain the wurtzite structure, which is also the thermodynamically most stable phase for the bulk. Therefore, the zinc oxide is modeled by clusters (see Figs. 1b and 1d) cleaved from the bulk with distinct facets corresponding to the specific surface orientations: (100), (110), and (001), as shown in Fig. 2. The atomic coordinates are taken from experimental lattice parameters.[22] Both the (100) and (110) surfaces are non-polar surfaces with the same number of Zn and O atoms on a single plane, while the (001) surface is highly polarized with either Zn- or O- terminated surfaces. In the following study, we have considered both terminations for a (001) surface. The Zn/O-terminated (001) surface can exist in both (1×1) bulk-like termination[23,24] and a reconstructed surface structure.[25,26] Note that in the cluster model, we did not take into account the surface relaxation and reconstruction, but rather focused on the generic effect of unique atomic arrangement along different surface orientations. The larger cluster

$Zn_{15}O_{15}$, containing four bilayers along the [001] direction was used together with the larger cluster model of graphene ($C_{54}H_{18}$) to test the size effect of the cluster model. The interaction of Zn-terminated (001) surface with graphene was also carried out via a slab model for comparison of results by applying the periodic boundary conditions (PBC),[27] where 3×3 ZnO (001) surface is matched with 4×4 Graphene (see Figs. 1e and 1f) with a lattice mismatch less than 2%. The ZnO slab contains four bilayers to eliminate the effect from the far-side surface. The plane wave basis sets and the PAW-PBE functional[28] with van der Waals corrections[29] were used.

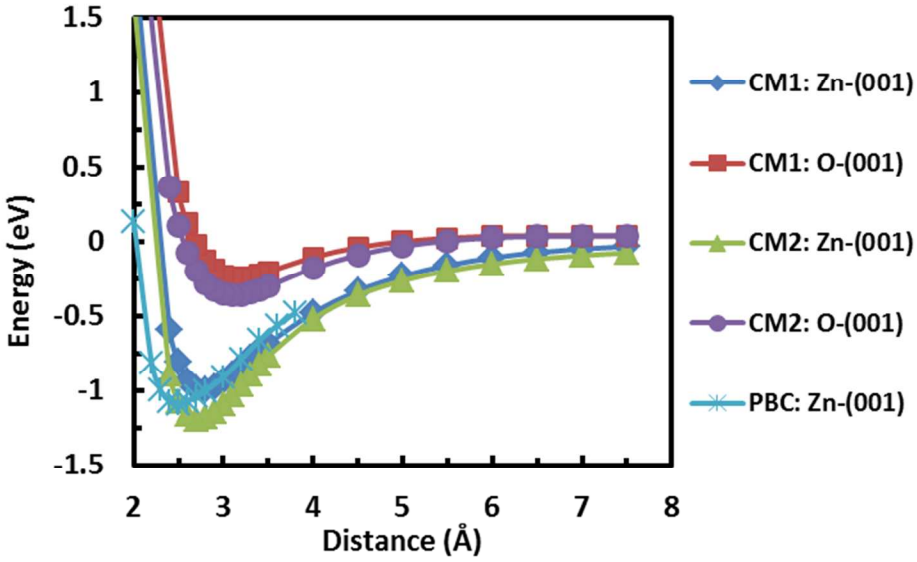

FIG. 3. Comparison of potential energy curves of ZnO interacting with graphene from O-terminated (001) and Zn-terminated (001) surfaces using different computational models, the small cluster model (CM1), the larger cluster model (CM2) and the slab model (PBC). The PBC results are scaled by a factor of 3 since the slab contains three times of ZnO pairs as the cluster.

The potential energy surface (PES) is scanned while bringing the ZnO cluster incrementally closer to graphene with the targeted surface of the ZnO cluster parallel to the graphene. The step size of the scan varies from 0.5 to 0.1 Å in order to efficiently locate the energy minimum on the PES. The interfacial binding strength is calculated by taking the energy difference between the sum of energies of the isolated graphene and the ZnO cluster, and the total energy of the combined system at the equilibrium position when the total energy of the system is a minimum. To first validate our model, we have compared the

results of the PESs for graphene interacting with Zn-terminated and O-terminated (001) surfaces using different models, as shown in Fig. 3. The results are in fairly good agreement among the small cluster model (CM1), the larger cluster model (CM2) and the slab model (PBC) with a difference in binding energy less than 0.2 eV. Different surface orientations and surface binding sites are sampled including the most typical atop, bridge and hole (at the center of the hexagon ring) sites. All the rest of reported results are based on CM1, if not otherwise indicated.

All the calculations were done within the framework of DFT as implemented in the Gaussian09 program,[30] which allows an accurate account of the charge redistribution at the atomic level due to the interaction between ZnO and graphene. The hybrid exchange-correlation functional B97-1 [31] was chosen for the calculation. This functional was parameterized to the energetic data of the G2 training set via a self-consistent procedure. It yields more accurate energetics and better geometries than the B3LYP functional.[31] The B97-1 functional also has a good account of the van der Waals interactions, as shown in the study of rare-gas dimers, alkaline-earth metal dimers, the zinc dimer, and zinc-rare gas dimers.[32] The comparison of results using different functional forms is listed in the Supplemental Materials Table S1. It appears that all the chosen functional forms give consistent trends in the variation of interfacial binding energies, while the B97-1 functional produces better overall agreement with experiment. The 6-31G(d) basis sets were used for C, O and H, and the LanL2DZ effective core potential and basis set was used for Zn.

III. RESULTS AND DISCUSSION

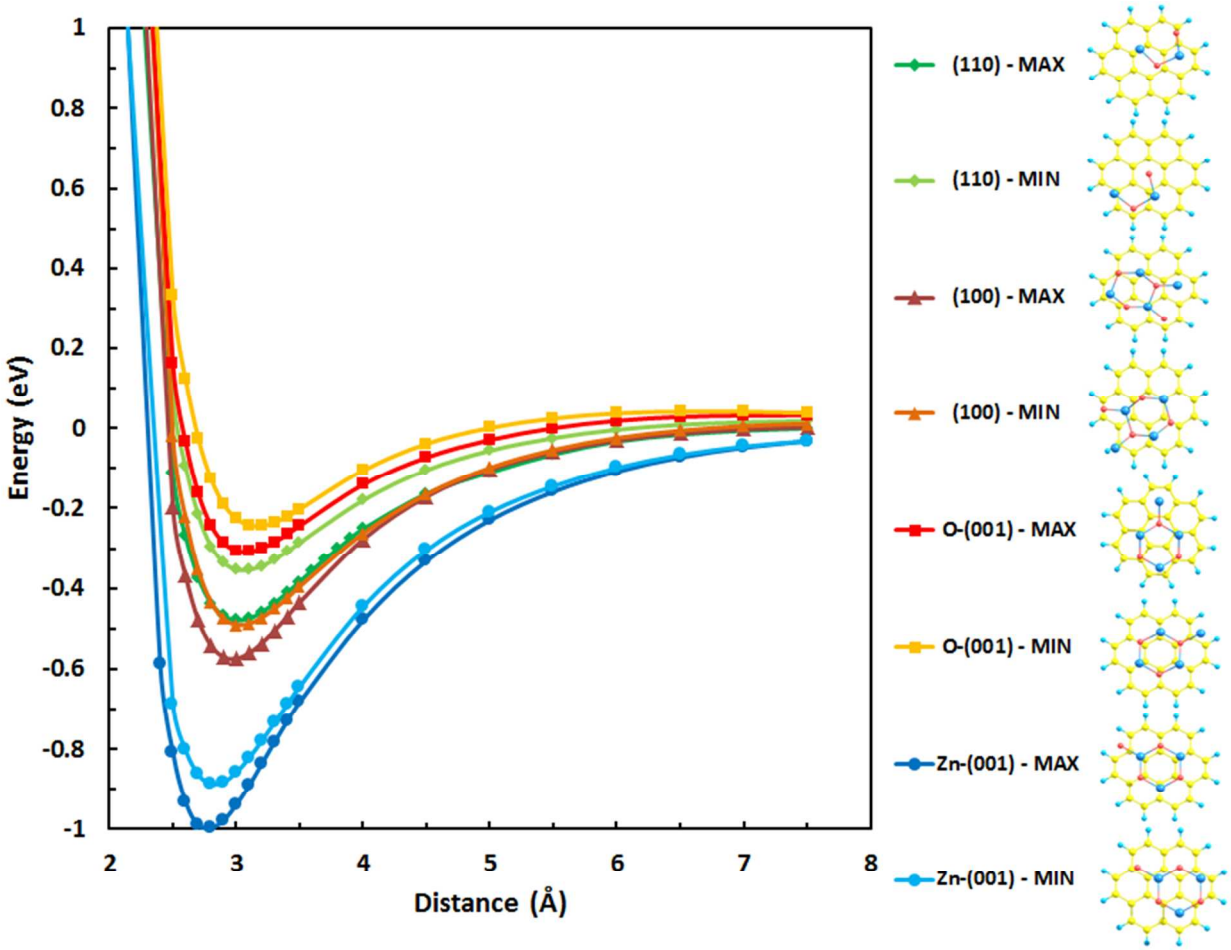

FIG. 4. Potential energy curves of ZnO interacting with graphene from (110), (100), O-terminated (001) and Zn-terminated (001) surfaces. Representative binding sites are shown for the maximum and minimum interfacial binding strengths for each of the surfaces. Only the bottom layer of ZnO at the interface is shown for clarity.

Potential energy surfaces were scanned as the ZnO cluster was vertically brought closer to graphene along different directions. Graphene is kept fixed at optimized positions, since it has been previously shown that the deformation of graphene is negligibly small.[13,14] Each path is varied by the ZnO surface orientation facing graphene and the landing sites on graphene. Graphene has three typical sites: the atop site right above a C atom, the bridge site between two C atoms and the hole site above the center of the C hexagonal ring. The facets of the ZnO cluster feature undercoordinated Zn and O atoms, namely two-fold Zn (Zn^{I}), three-fold Zn (Zn^{II}), two-fold O (O^{I}), and three-fold O (O^{II}), as shown in Fig. 2. We have considered different types of Zn and O atoms binding at different sites of graphene in each potential

energy scan. Representative potential energy curves are plotted in Fig. 4 for the strongest and weakest binding for each of the surface orientations, together with illustrations of the binding configurations. A full summary of all the binding sites considered, and the potential energy curves, the binding energies and equilibrium distances calculated is provided in the Supplemental Materials: Fig. S1-S3.

Table 1 Calculated highest and lowest interfacial binding energies E_b, equilibrium distance R_0 and adhesive energies E_{adh} for each surface orientation.

Surface	Highest Binding Strength			Lowest Binding Strength		
	R_0 (Å)	E_b (eV)	E_{adh} (J/m^2)	R_0 (Å)	E_b (eV)	E_{adh} (J/m^2)
110	3.0	0.48	0.262	3.1	0.35	0.191
100	3.0	0.57	0.270	3.0	0.49	0.232
O-terminated 001	3.1	0.31	0.181	3.2	0.24	0.140
Zn-terminated 001	2.8	1.00	0.583	2.8	0.89	0.519

All the potential energy curves demonstrate a similar shape. The energy starts from a plateau as ZnO and graphene are far from each other, and monotonically decreases to a minimum at the equilibrium distance R_0, and then increases drastically as ZnO gets closer to graphene. The calculated equilibrium distance R_0, and binding energy E_b, for each case are presented in Table 1 (See Supplemental Materials: Table S2-S4 for full details of all surface calculations). The equilibrium distance R_0 is mostly near 3.0 Å with an exception of the strongest binding Zn-terminated (001) surface (2.8 Å) and the weakest binding O-terminated (001) surface (3.2 Å). For the same surface orientation, only slight variation (~0.1 eV) in binding energy is observed for different binding sites and Zn/O atoms with different coordination numbers (Zn^I vs. Zn^{II}; O^I vs. O^{II}), as is clearly shown from the results of (110) and (100) surfaces. The same has been observed in previous studies of Zn/O-terminated (001) surfaces.[14] Overall, Zn prefers atop and bridge sites while O prefers hole sites; the 2-fold Zn/O has slightly higher binding energy than the 3-fold Zn/O. The interaction therefore has little dependence on the relative position of Zn/O with C atoms, indicating that the binding does not purely originate from van der Waals dispersion interaction. Nor does it have a noticeable dependence on the coordination number of Zn/O atom, as an indicator of chemical interaction.

Instead, we have observed that the calculated binding energy strongly depends upon the surface orientation and termination of ZnO, decreasing in the order of Zn-terminated (001) > (100) > (110) > O-terminated (001). The most favorable interaction orientation was therefore determined to be the Zn-terminated (001) surface. This is also the most commonly studied surface for ZnO for its interaction with other materials. For the same type of polar surfaces, when changing the surface termination from Zn to O, the binding energy is greatly reduced. The same trend was reported previously using a periodic slab model.[13] The π electrons of graphene hexagons demonstrate a more favorable deformation responding to the positively charged Zn ions, which has a much lower electronegativity (1.65) than O (3.44). These results are broadly consistent with the surface energies, where the Zn-terminated (001) surface is more active and unstable, and produces a stronger interaction than the O-terminated (001) surface.[33]

To better compare the interfacial binding strength for different surface orientations of ZnO and to compare with experimental values, we have further calculated the surface density of Zn-O atomic pairs and the interfacial adhesive energy E_{adh},*i.e.* binding energy per unit surface area (see details in the Supplemental Materials) , also listed in Table 1. The order of E_{adh} remains the same as the calculated E_b, with the value of the (110) surface getting much closer to that of the (100) surface owing to the higher surface density of Zn-O pairs on (110) (~7 pairs per 100 Å^2) than on (100) (~6 pairs per 100 Å^2). The (001) surface is by far the most closely packed surface with a surface density of 11 pairs of Zn-O per 100 Å^2. Adhesive energy is consistent with the surface energy of ZnO by following the same order. In addition, it is worth noting that the calculated adhesive energy is on average in good agreement with the value (0.261±0.054 J/m^2) measured by the atomic force microscopy (AFM) lift-off of a ZnO-coated tip from highly oriented pyrolytic graphite,[12] considering that no specific information is given about the surface orientation of the ZnO film in the experiment.

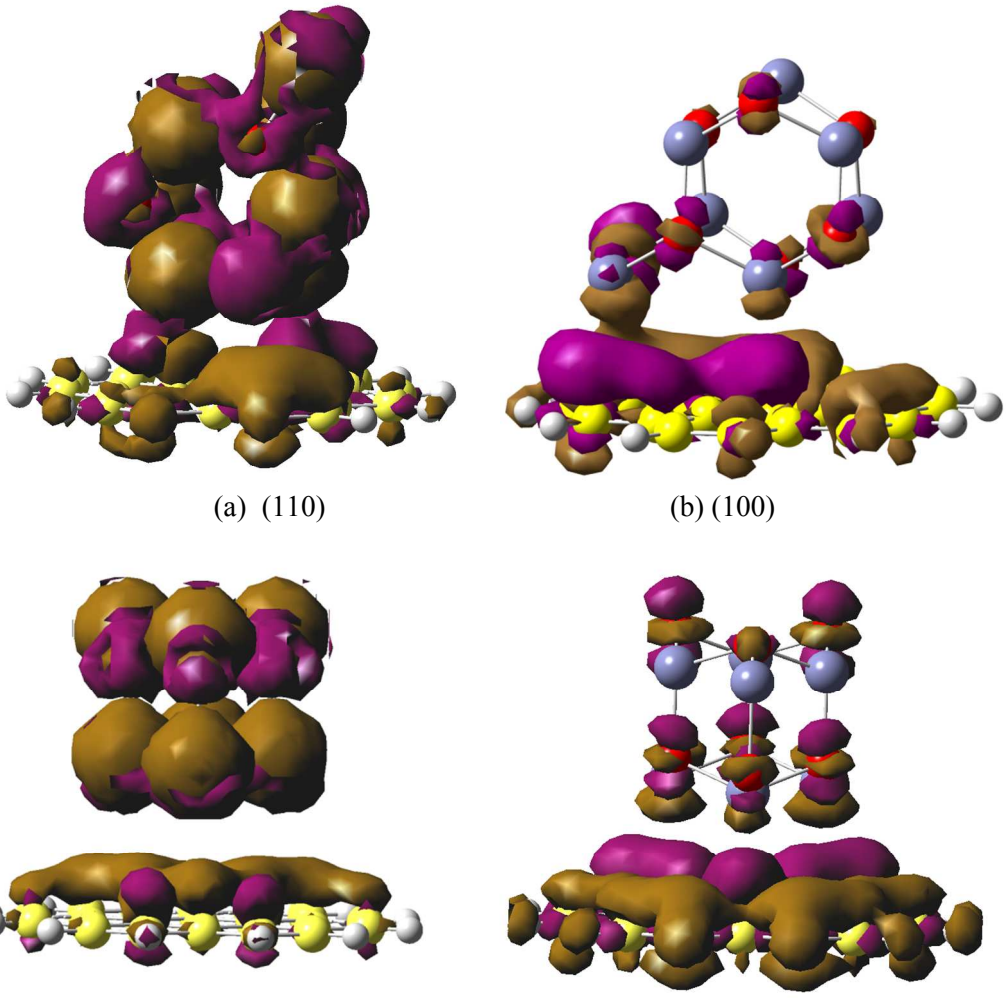

(a) (110) (b) (100)

(c) O-terminated (001) (d) Zn-terminated (001)

FIG 5. Difference charge density plots for graphene interacting with ZnO along (a) (110), (b) (100), (c) O-terminated (001) and (d) Zn-terminated (001) ZnO surfaces. The isosurface value is taken to be 0.0006 a.u. and golden surfaces represent electron deficiency (+); purple surfaces represent electron excess (-).

The highest binding energy per Zn-O pair is calculated to be 0.24, 0.28, 0.10, 0.33eV for (110), (100), O-terminated (001) and Zn-terminated (001) ZnO surfaces, respectively. In order to understand the difference in the interfacial binding strength demonstrated for different surface orientations of ZnO, we plot the difference charge density as defined below for all the four strongest binding configurations (Fig. 5).

$$\Delta\rho = \rho_{\mathrm{ZnO\cdots Graphene}} - (\rho_{\mathrm{ZnO}} + \rho_{\mathrm{Graphene}}) \qquad (1)$$

Where ρ_{ZnO}, $\rho_{Graphene}$, and $\rho_{ZnO\cdots Graphene}$ are the electron density of ZnO, graphene and the combined system, respectively.

From Fig. 5, we can see significant charge redistribution in ZnO and graphene attributed to the interaction, while negligible charge transfer is found between ZnO and graphene (see Supplemental Materials: Table S5 and Fig. S4). The charge redistributions induced by the intrinsic electric dipole of ZnO on different surfaces provide a possible understanding of the associated interaction strength. The (001) surface has the largest dipole moment (5.05 Debye) along the vertical (out-of-plane) direction. The Zn-terminated polar surface induces a dipole in the charge distribution of graphene (Fig. 5d) that was much larger than the O-terminated polar surface (Fig. 5c). The non-polar (100) surface has a large dipole moment (9.31 Debye) as well, but it is in-plane. It still causes significant charge redistribution in graphene as shown in Fig. 5b. But the energy gain is less compared to the Zn-terminated (001) surface. The (110) surface has a typical quadrupole and only a small net in-plane dipole, leading to a relatively small electron density deformation in graphene, but a noticeable charge redistribution in ZnO itself (Fig. 5a). The induced polarity without an apparent evidence of charge transfer indicates that the interfacial forces are primarily due to dipole-induced dipole interactions instead of chemical interactions. This finding is consistent with the fact that graphene has a high polarizability owing to its highly delocalized π electrons.

IV. CONCLUSIONS

We have done a systematic study of the interactions between graphene and different surfaces of ZnO based on a first-principles approach. The calculated interfacial binding strength strongly depends upon the ZnO surface orientation and termination. Of the different orientations, there is, however, only slight variation in binding energy due to different binding sites and Zn/O atoms with different coordination numbers. The charge redistribution due to the interaction is significant, while there is little charge transfer

between the ZnO and graphene. The difference in the interfacial binding energy of different surfaces to graphene is traced back to the intrinsic difference in their ionic configuration of each surface and thereby unique electric dipole distributions. The generic dipole of the ZnO surface can then cause charge redistribution in graphene and produce an induced dipole. The dipole-induced dipole interaction is the primary source of interaction between ZnO and graphene. The interfacial binding strength follows the order of Zn-terminated (001) > (100) > (110) > O-terminated (001), as a reflection of the in-plane, out-of-plane dipole moment of the surface layer of the oxide. This finding could generally be applied to other ionic crystals interacting with graphene as well. Our calculated binding energies are comparable to the experimentally measured value.

In the hybrid carbon fiber reinforced polymer composites, the binding of ZnO nanowires with carbon fibers are critical to form a uniform and stable interphase to achieve enhanced interfacial shear strength and tensile strength. The results of these calculations suggest that some surface has stronger binding than the other. It may provide guidelines with the preferable growing/exposing surface orientation. On the other hand, the overall small adhesion energy of pristine graphene with ZnO indicates that the introduction of chemical functional groups through graphene oxidation or other surface treatment is very necessary to substantially improve the interface adhesion strength with ionic crystals. The interface adhesion strength between nano ionic interphase with functionalized graphene are our on-going research.

.

ACKNOWLEDGMENTS

H.H. wishes to thank Valparaiso University for the Faculty Start-up Funds and the grant of computer time from Argonne Center for Nanoscale Materials. Technical support from P. Nord is gratefully acknowledged.

REFERRENCES:

(1) Lin, Y.; Ehlert, G.; Sodano, H. A. *Advanced Functional Materials* **2009**, *19*, 2654.
(2) Li, B.; Cao, H. *Journal of Materials Chemistry* **2011**, *21*, 3346.
(3) Zhang, N.; Zhang, Y.; Xu, Y.-J. *Nanoscale* **2012**, *4*, 5792.
(4) Zhang, N.; Yang, M.-Q.; Tang, Z.-R.; Xu, Y.-J. *ACS Nano* **2014**, *8*, 623.
(5) Lee, J. M.; Pyun, Y. B.; Yi, J.; Choung, J. W.; Park, W. I. *Journal of Physical Chemistry C* **2009**, *113*, 19134.
(6) Chen, J.; Li, C.; Eda, G.; Zhang, Y.; Lei, W.; Chhowalla, M.; Milne, W. I.; Deng, W.-Q. *Chemical Communications* **2011**, *47*, 6084.
(7) Kim, M. K.; Yi, D. K.; Paik, U. *Langmuir* **2010**, *26*, 7552.
(8) Chang, H.; Sun, Z.; Ho, K. Y.-F.; Tao, X.; Yan, F.; Kwok, W.-M.; Zheng, Z. *Nanoscale* **2011**, *3*, 258.
(9) Dong, X.; Cao, Y.; Wang, J.; Chan-Park, M. B.; Wang, L. H.; Huang, W.; Chen, P. *RSC Advances* **2012**, *2*, 4364.
(10) Ali, A.; Jo, J.; Yang, Y. J.; Choi, K. H. *Applied Physics A* **2014**, *114*, 323.
(11) Nam, G.; Baek, S.; Cho, C.; Park, I. *Nanoscale* **2014**, *6*, 11653.
(12) Galan, U.; Sodano, H. A. *Applied Physics Letters* **2012**, *101*, 151603.
(13) Geng, W.; Zhao, X.; Liu, H.; Yao, X. *Journal of Physical Chemistry C* **2013**, *117*, 10536.
(14) Xu, P.; Tang, Q.; Zhou, Z. *Nanotechnology* **2013**, *24*, 305401.
(15) Wang, R. C.; Liu, C. P.; Huang, J. L.; Chen, S.-J.; Tseng, Y.-K.; Kung, S.-C. *Applied Physics Letters* **2005**, *87*, 013110.
(16) Yang, P.; Yan, H.; Mao, S.; Russo, R.; Johnson, J.; Saykally, R.; Morris, N.; Pham, J.; He, R.; Choi, H. J. *Advanced Functional Materials* **2002**, *12*, 323.
(17) Huang, M. H.; Mao, S.; Feick, H.; Yan, H.; Wu, Y.; Kind, H.; Weber, E.; Russo, R.; Yang, P. *Science* **2001**, *292*, 1897.
(18) Tian, Z. R.; Voigt, J. A.; Liu, J.; Mckenzie, B.; Mcdermott, M. J.; Rodriguez, M. A.; Konishi, H.; Xu, H. *Nature Materials* **2003**, *2*, 821.
(19) Wang, Z. L.; Kong, X. Y.; Ding, Y.; Gao, P.; Hughes, W. L.; Yang, R.; Zhang, Y. *Advanced Functional Materials* **2004**, *14*, 943.
(20) Na, S.-H.; Park, C.-H. *Journal of the Korean Physical Society* **2009**, *54*, 867.
(21) Ren, C.; Yang, B.; Wu, M.; Xu, J.; Fu, Z.; lv, Y.; Guo, T.; Zhao, Y.; Zhu, C. *Journal of Hazardous Materials* **2010**, *182*, 123.
(22) Karzel, H.; Potzel, W.; Kofferlein, M.; Schiessl, W.; Steiner, M.; Hiller, U.; Kalvius, G. M. *Physical Review B* **1996**, *53*, 11425.
(23) Dulub, O.; Boatner, L. A.; Diebold, U. *Surface Science* **2002**, *519*, 201.
(24) Lindsay, R.; Muryn, C. A.; Michelangeli, E.; Thornton, G. *Surface Science* **2004**, *565*, L283.
(25) Kunat, M.; Girol, S. G.; Burghaus, U.; Woll, C. *Journal of Physical Chemistry B* **2003**, *107*, 14350.
(26) Heiland, G.; Kunstmann, P. *Surface Science* **1969**, *13*, 72.
(27) Kresse, G.; Furthmuller, J. *Physical Review B* **1996**, *54*, 11169.
(28) Perdew, J. P.; Burke, K.; Ernzerhof, M. *Physical Review Letters* **1996**, *77*, 3865.
(29) Grimme, S. *Journal of Computational Chemistry* **2006**, *27*, 1787.
(30) Frisch, M. J. T., G. W.; Schlegel, H. B.; Scuseria, G. E.; Robb,; M. A.; Cheeseman, J. R. M., J. A., Jr.; Vreven, T.; Kudin, K. N.;; Burant, J. C. M., J. M.; Iyengar, S. S.; Tomasi, J.; Barone, V.;; Mennucci, B. C., M.; Scalmani, G.; Rega, N.; Petersson, G. A.;; Nakatsuji, H. H., M.; Ehara, M.; Toyota, K.; Fukuda, R.; Hasegawa, J.;; Ishida, M. N., T.; Honda, Y.; Kitao, O.; Nakai, H.; Klene, M.; Li,; X.; Knox, J. E. H., H. P.; Cross, J. B.; Bakken, V.; Adamo, C.;; Jaramillo, J. G., R.; Stratmann, R. E.; Yazyev, O.; Austin, A. J.;; Cammi, R. P., C.;

Ochterski, J. W.; Ayala, P. Y.; Morokuma, K.;; Voth, G. A. S., P.; Dannenberg, J. J.; Zakrzewski, V. G.; Dapprich,; S.; Daniels, A. D. S., M. C.; Farkas, O.; Malick, D. K.; Rabuck, A. D.;; Raghavachari, K. F., J. B.; Ortiz, J. V.; Cui, Q.; Baboul, A. G.;; Clifford, S. C., J.; Stefanov, B. B.; Liu, G.; Liashenko, A.; Piskorz,; P.; Komaromi, I. M., R. L.; Fox, D. J.; Keith, T.; Al-Laham, M. A.;; Peng, C. Y. N., A.; Challacombe, M.; Gill, P. M. W.; Johnson,; B.; Chen, W. W., M. W.; Gonzalez, C.; Pople, J. A. ; Pittsburgh, PA: Gaussian: 2009.

(31) Hamprecht, F. A.; Cohen, A.; Tozer, D. J.; Handy, N. C. *Journal of Chemical Physics* **1998**, *109*, 6264.

(32) Zhao, Y.; Truhlar, D. G. *Journal of Physical Chemistry A* **2006**, *110*, 5121.

(33) Zhang, Y.; Guo, Z.; Gao, X.; Cao, D.; Dai, Y.; Zhao, H. *Journal of Semiconductors* **2010**, *31*, 082001.